Enhanced low-field magnetization and magnetoresistance in nano-MgO added $La_{2/3}Ca_{1/3}MnO_3$ composites

2007 J. Phys. D: Appl. Phys. 40 3300

(http://iopscience.iop.org/0022-3727/40/11/007)

IOP Publishing Journal of Physics D: Applied Physics
J. Phys. D: Appl. Phys. **40** (2007) 3300–3305 doi:10.1088/0022-3727/40/11/007

Enhanced low-field magnetization and magnetoresistance in nano-MgO added $La_{2/3}Ca_{1/3}MnO_3$ composites

Zhigao Sheng[1], Yuping Sun[1], Xuebin Zhu[1], Wenhai Song[1] and Peng Yan[2]

[1] Key Laboratory of Materials Physics, Institute of Solid State Physics and Hefei High Magnetic Field Laboratory, Chinese Academy of Sciences, Hefei 230031, People's Republic of China
[2] Binzhou Medical College, Yantai 264003, People's Republic of China

E-mail: ypsun@issp.ac.cn

Received 18 January 2007, in final form 29 March 2007
Published 18 May 2007
Online at stacks.iop.org/JPhysD/40/3300

Abstract
We report the significant enhancement of low-field magnetization and magnetoresistance (MR) in $La_{2/3}Ca_{1/3}MnO_3$ (LCMO) compounds with 5 at.% nano-MgO addition in the form of both nanoparticle and nanowire. It is found that the magnetization of the nano-MgO added compounds is highly sensitive to a low applied field below 7 kOe compared with the MgO-free LCMO. In addition, the enhancement of low-field MR is found in nano-MgO added compounds and the enhancement for the nanowire MgO-added composite is more remarkable than that for the nanoparticle MgO-added one. Moreover, two ferromagnetic phases with low-T_C and high-T_C in nano-MgO added compounds are observed. These results demonstrate that the low-field transport and magnetic properties of LCMO compounds can be effectively manipulated by controlling the morphology and dispersion of the insulating barrier using nano-MgO addition.

1. Introduction

The discovery of 'colossal magnetoresistance' (CMR) in manganite-based compounds has caused intense research activities over the last few years [1–3]. However, the intrinsic CMR effect is only triggered at high magnetic fields of several tesla, which restrains its use for practical applications. For most applications one needs magnetoresistance (MR) at low values of the field. To this end, another property of CMR manganites, namely the large spin polarization below the ferromagnetic (FM) transition temperature (T_C), can be utilized in the form of spin-polarized tunnelling through CMR/insulator/CMR structures to enhance the low-field magnetoresistance (LFMR) in these materials. Recently, several groups have attempted to enhance the MR by making CMR–insulator composites, which naturally contain CMR/insulator/CMR boundaries in their bulk form. For example, $La_{0.7}Sr_{0.3}MnO_3$–CeO_2 composites [4] and $La_{0.7}Ca_{0.3}MnO_3$–$SrTiO_3$ composites [5] as well as $La_{0.7}Ca_{0.3}MnO_3$ films containing MgO as the insulating boundary [6] have been reported earlier. In such a system, the enhancement of LFMR can also be commonly explained by the model of spin-polarized tunnelling taking place across interfaces or grains with insulator layers as barriers [7, 8]. On the basis of this model, the efficiency of insulator barriers, in these chemical phase separation systems, is very important for the enhancement of LFMR. Therefore, efforts to control the parameter and the scale of insulator barrier would be worth considering to enhance LFMR.

The research into nano-structure materials became all the more attractive in recent years for they exhibit fundamentally different properties from those of conventional polycrystals with the same composition [9]. Hence, one may anticipate that the small size and large aspect ratio of nano-structure insulator materials would enhance the efficiency of insulator barriers and thus the magnetic and electrical properties of nano-structure

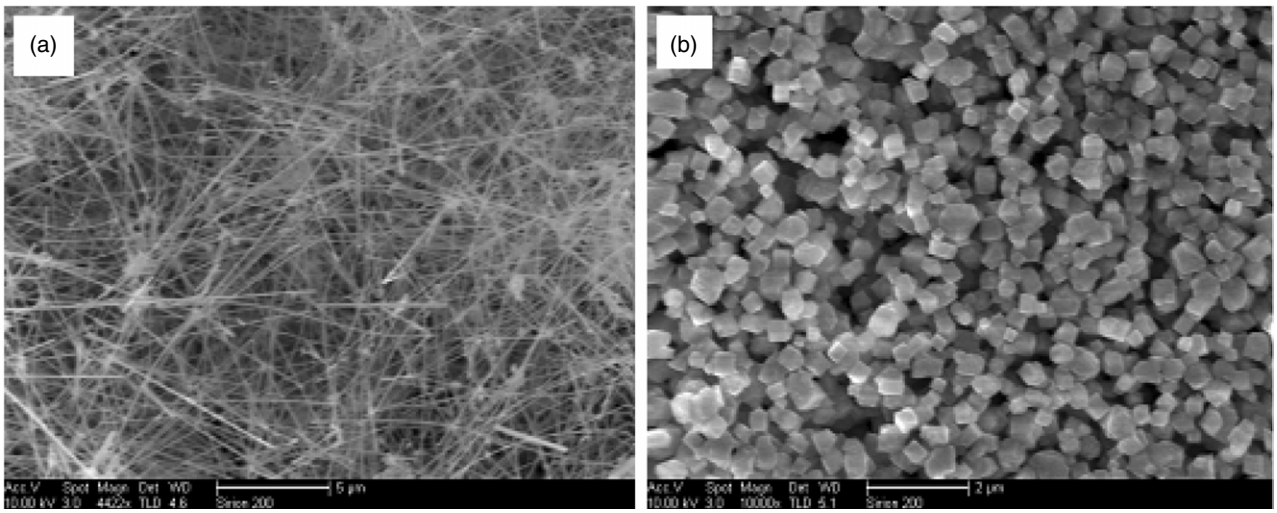

Figure 1. SEM images of as-synthesized (*a*) nanowires and (*b*) nanoparticles of MgO.

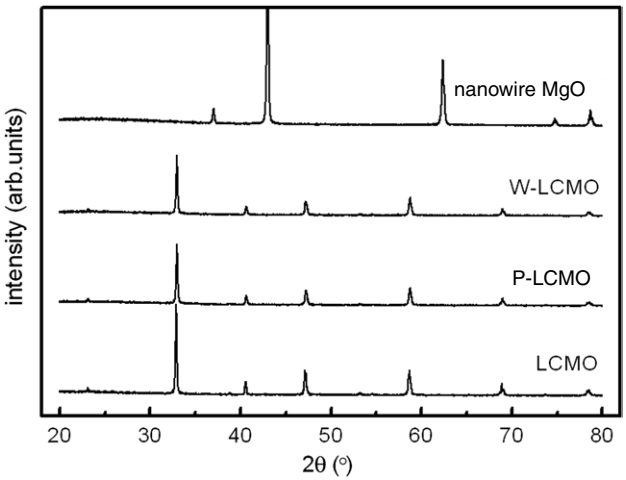

Figure 2. X-ray diffraction patterns of the nanowire MgO, W-LCMO, P-LCMO and LCMO samples.

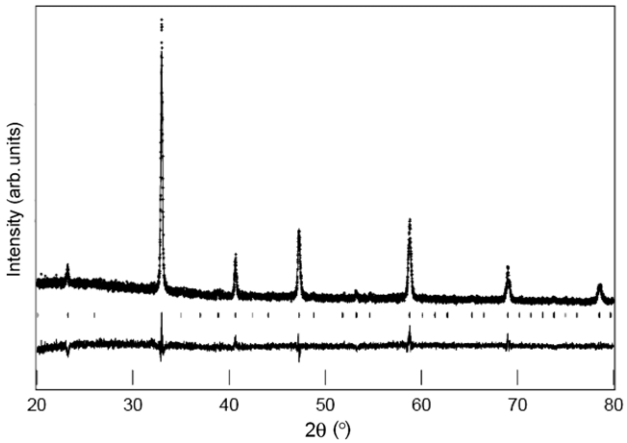

Figure 3. The experimental and calculated XRD patterns of the P-LCMO sample. Crosses indicate the experimental data and the calculated data is the continuous line overlapping them. The lowest curve shows the difference between experimental and calculated patterns. The vertical bars indicate the expected reflection positions.

insulator added CMR composites. In this work, we report the enhanced low-field magnetization and magnetoresistance of nano-MgO added $La_{2/3}Ca_{1/3}MnO_3$ (LCMO) composites. It reveals that the efficiency of artificial insulator barriers could be much enhanced by using low-dimension nano-materials.

2. Experimental

Nano-MgO including nanoparticles and nanowires and pure LCMO composites were prepared as indicated in [10, 11], respectively. Pure LCMO powder and nano-MgO were mixed in the weight ratio 0.95 : 0.05 and then heated at 850 °C in air atmosphere in order to make a good connection between adjacent LCMO particles and nano-MgO. All the samples are prepared using the same process to ensure the same grain size of LCMO particles. The nanoparticle MgO and nanowire MgO-added LCMO composites are written as P-LCMO and W-LCMO, respectively. The structure and phase purity of the composites were checked by means of x-ray diffraction (XRD) at room temperature. High-resolution field emission scanning electron microscopy ((FE-SEM), Sirion 200, FEI) with an energy x-ray microanalysis system ((EDX), INCA, Oxford) was utilized to check the composition and microstructure of the samples. The temperature dependences of the resistance of samples under zero and an applied field were measured by the standard four-probe method from 5 to 390 K on a Quantum Design physical property measurement system (PPMS) (1.9 K $\leqslant T \leqslant$ 400 K, 0 T $\leqslant H \leqslant$ 9 T). The magnetization of samples was measured on a Quantum Design superconducting quantum interference device (SQUID) MPMS system (1.9 K $\leqslant T \leqslant$ 400 K, 0 T $\leqslant H \leqslant$ 5 T).

3. Results and discussion

Typical FE-SEM images of the as-synthesized MgO nanowires and nanoparticles are shown in figures 1(*a*) and (*b*), respectively. It can be seen that both nanowires and nanoparticles exhibit a small size distribution. The diameter

Table 1. Refined structural parameters for all samples at room temperature. Both d_{Mn-O} and $\theta_{Mn-O-Mn}$ are average values calculated from refined results. Digits in parentheses are statistical errors of the last significant digit.

Sample	a (Å)	b (Å)	c (Å)	d_{Mn-O} (Å)	$\theta_{Mn-O-Mn}$ (deg)	χ^2
LCMO	5.4566(6)	5.45114(8)	7.7075(5)	1.9498(3)	164.39(5)	1.898
P-LCMO	5.4542(2)	5.4641(2)	7.7081(6)	1.9510(7)	162.87(1)	1.676
W-LCMO	5.4492(1)	5.4609(1)	7.7124(7)	1.9509(8)	162.87(5)	1.761

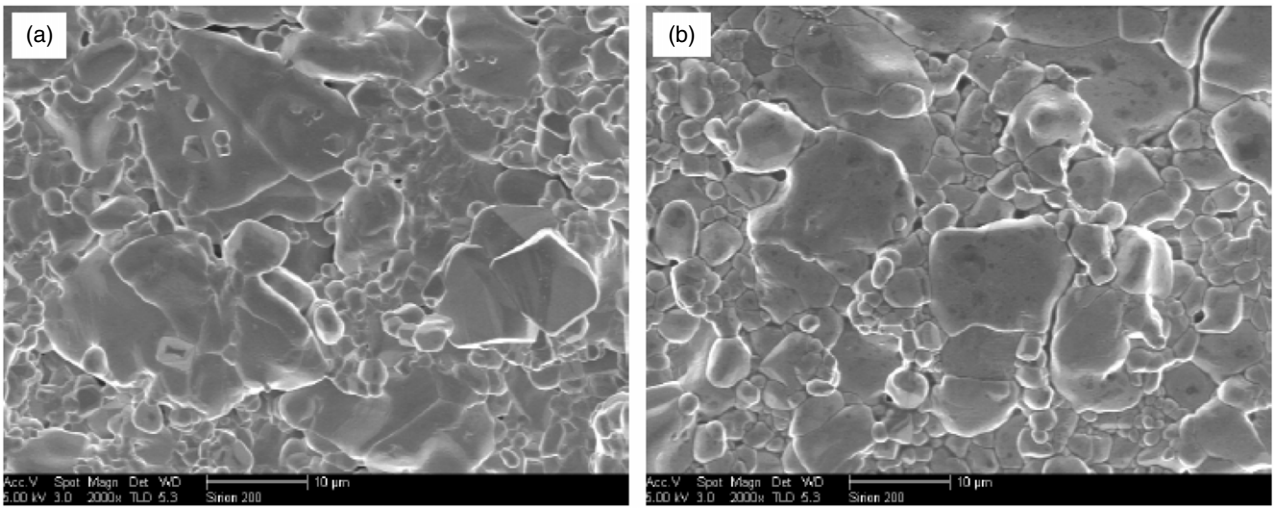

Figure 4. SEM images of (*a*) W-LCMO and (*b*) P-LCMO.

of nanowires is approximately 100 nm and the edge length of a nanoparticle of cubic shape is about 200 nm. When the LCMO and nano-MgO are ground, then pelletized and heated, nano-MgO will locate at grain boundaries of LCMO and form a very thin insulating barrier around the LCMO domains due to the large aspect ratio of nano-MgO and the lower energy barrier of the LCMO grain boundary. In addition, it is also reasonable to assume that most of the LCMO grains can be surrounded by nano-MgO based on being the relation between the aspect ratios of LCMO, nanoparticle MgO and nanowire MgO as 95 : 70.1 : 93.7 obtained from the proportion (0.95 : 0.05) of LCMO and nano-MgO and their morphologies. Therefore, compared with MgO nanoparticle, the efficiency is higher for nanowire MgO to disperse between LCMO grains as the insulating barrier from the theoretical calculation.

Figure 2 shows the XRD patterns of nanowire MgO, W-LCMO, P-LCMO and LCMO samples. It exhibits that the XRD pattern of all the nano-MgO added LCMO samples is similar to that of the sample without addition, implying that no structure change occurs. Moreover, the secondary phase of 5 at.% added MgO is undetectable in the XRD pattern of nano-MgO added LCMO samples. All x-ray diffraction data of nano-MgO added LCMO are refined to *Pbnm* symmetry using the Rietveld method [11]. As typical results, figure 3 shows the experimental and calculated XRD patterns for the P-LCMO sample. It shows that the results of fitting are quite good. The obtained structural parameters are listed in table 1. It is found that the lattice parameters are elongated by nano-MgO addition. Moreover, the average Mn–O–Mn bond angle decreases and the average Mn–O bond length increases with nano-MgO addition, which is suggested to come from the tensile strain caused by MgO. The SEM pictures for W-LCMO and P-LCMO samples are shown in figure 4. It can be seen that they are similar to each other and it is hard to find MgO composition in the SEM picture.

In order to confirm that nano-MgO added LCMO composites consist of two separated LCMO and MgO phases, the line-scanned spatial fluctuation of elements La, Mn and Mg across the grain boundary of LCMO is performed using an EDX analysis accompanied by FE-SEM. As an example, the SEM image of P-LCMO and the line-scanned spatial fluctuation of elements La, Mn and Mg (figures 5(*b*), 2(*c*) and (*d*)) are shown in figure 5(*a*)–(*d*). The line-scan measurement was done along the black line as plotted in figure 5(*a*). It is obvious that the as-probed spatial distributions of La and Mn show synchronous variation in the measured range and have minimum values at the grain boundary. In contrast, the spatial distribution of Mg is opposite to that of La and Mn and has a peak in the vicinity of the grain boundary of LCMO. Although the data may only be semiquantitative, the present results demonstrate that the composite indeed consists of LCMO and MgO separated phases and nano-MgO locates at the LCMO grain boundaries acting as an insulating barrier.

The temperature dependences of the field-cooled (FC) magnetization (M) are shown in figure 6(*a*). As for pure LCMO sample, the Curie temperature T_C (defined as the one corresponding to the peak of dM/dT in the M versus T curves) is 265 K, which is comparable to the reported results [11]. However, compared with the MgO-free LCMO sample, nano-MgO added LCMO samples have two obvious magnetic transitions in the $M(T)$ curves as shown in figure 5(*a*). The first transition is located at $T_{C1}(= 265\,\mathrm{K})$, which is the same as the pure LCMO sample, while the second one T_{C2} is located at 199 K and 192 K for the P-LCMO and W-LCMO samples, respectively. The existence of double transition temperatures indicates that the nano-MgO added LCMO contains two FM

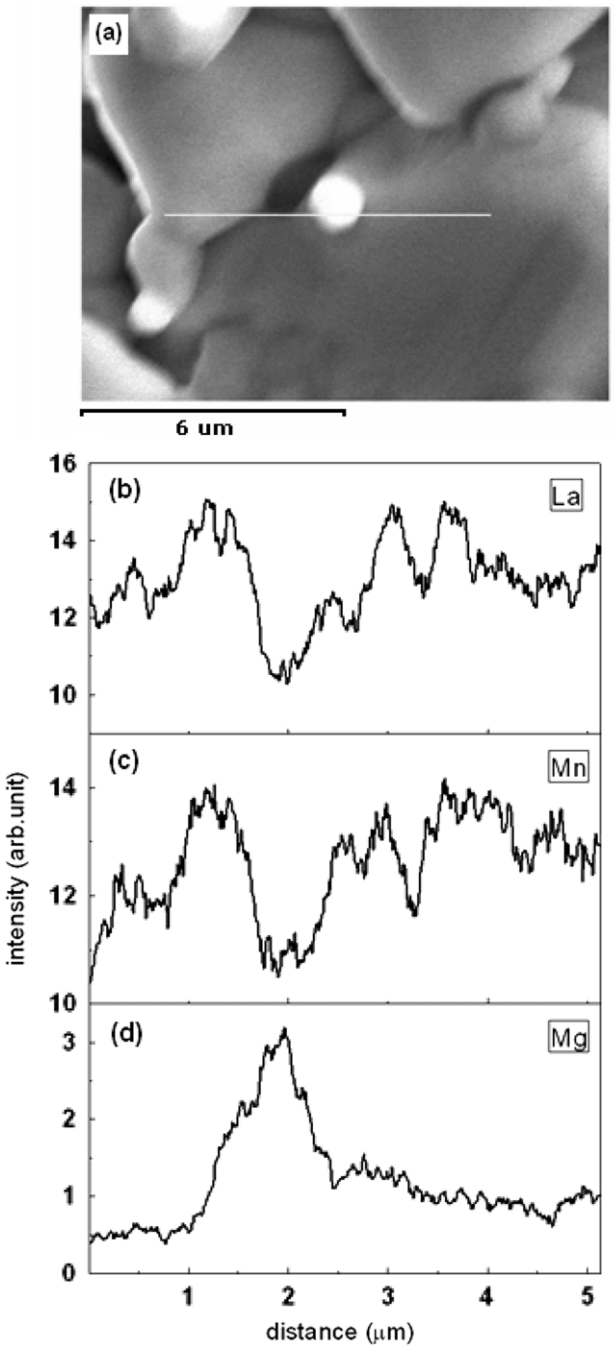

Figure 5. (*a*) SEM image of P-LCMO sample and EDX line-scanned profiles of elements La (*b*), Mn (*c*) and Mg (*d*) along the black line in the SEM image (*a*).

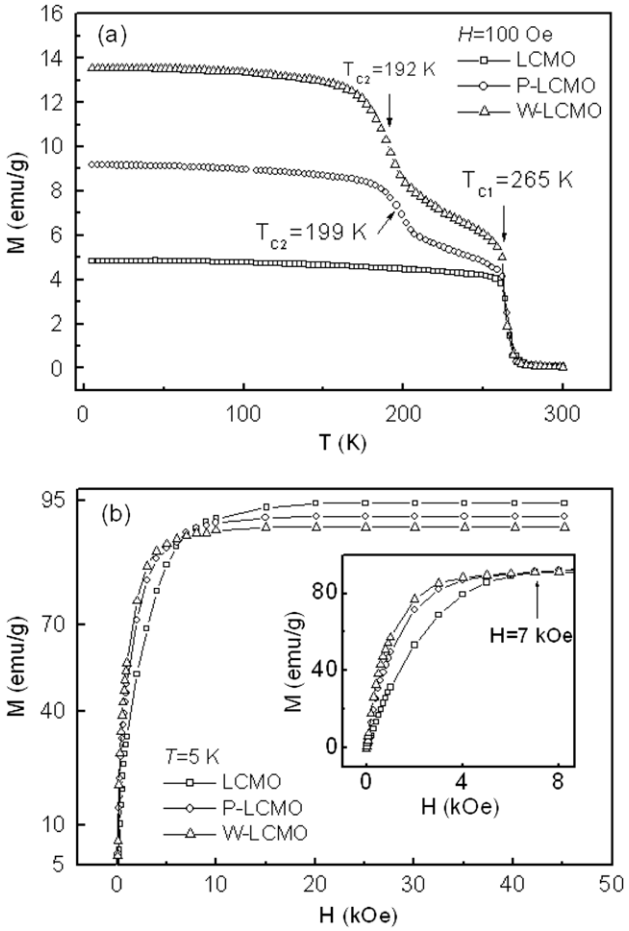

Figure 6. (*a*) The temperature dependence of magnetization M of nano-MgO added LCMO composites under FC mode at $H = 100$ Oe. (*b*) M as a function of magnetic field H at $T = 5$ K. The inset of (*b*) shows $M(H)$ below the field of 8 kOe.

phases, which is similar to the results with high MgO addition level manganite films reported by Moshnyaga *et al* [6], in which the lower temperature transition was explained by stress-induced nanoscale multiphase separation. As for our case, the nanoscale phase separation may also be the reason for double transitions in nano-MgO added LCMO composites. As mentioned above, LCMO domains with a mean diameter $D \sim 2.13\,\mu$m (see SEM in figure 5), separated by MgO, are probably magnetically decoupled. The size of the magnetic cluster, however, may be even smaller. As surrounded by the MgO, the nanoscale multiphase separation could possibly take place due to stress, which has been found at LCMO/$SrTiO_3$ interfaces [5]. Thus the double magnetic phases coexistence can be understood in the following way. As mentioned above, the MgO material with a cubic structure nearly acts as a matrix for LCMO growth inside the 'MgO box'. LCMO and MgO phases have a peculiar topology, as shown in figure 5, yielding a homogeneous 3D tensile stress distribution. Recently, Millis *et al* [12] asserted that the strain effect on T_C is attributed to two parts: the uniform bulk strain, ε_b, and the Jahn–Teller (J–T) strain, ε^*. The T_C can be expressed as

$$T_C(\varepsilon) = T_C(\varepsilon = 0)\left(1 - \alpha\varepsilon_b - \tfrac{1}{2}\Delta\varepsilon^{*2}\right), \qquad (1)$$

where $\alpha = 1/T_C(\mathrm{d}T_C/\mathrm{d}\varepsilon_b)$ and $\Delta = 1/T_C(\mathrm{d}^2T_C/\mathrm{d}^2\varepsilon^*)$. The magnitude of α and Δ represents the relative weight of the symmetry-conserving bulk strain and the symmetry-breaking J–T strain, respectively. The third term in equation (1) is related to the electron localization due to the splitting of the e_g level caused by the static J–T distortion and it is always negative [13]. The second term in equation (1) is related to the change in the kinetic energy of the carriers with respect to the strain. Since the ε_b can be either positive or negative depending on the sign of strain, this term can give either a negative or

positive contribution to the T_C. In our case, the misfit δ ($\approx$8%) between MgO and LCMO leads to an elongation of Mn–O–Mn (as shown in table 1) and a positive ε_b. Therefore, a larger bulk-strain effect on T_C can be interpreted as a hydrostatic expansion of the lattice, which increases the Mn–O–Mn distance and decreases the covalent mixing between the 3d-orbitals of Mn and those of 2p for oxygen. On the other hand, the 3D stress releases completely in the core of the LCMO grains and the T_C of these parts will be stable.

Another point worthy of special attention in figure 6(*a*) is that the magnetization of the P-LCMO and W-LCMO composites is larger than that of the MgO-free LCMO in the low field $H = 100$ Oe. Moreover, the low-field magnetization of the nanowire MgO-added composite is more remarkable than that of the nanoparticle MgO-added one. At $T = 230$ K the enhancement of magnetization (defined as $(M_{\text{MgO-doped}} - M_{\text{MgO-free}})/M_{\text{MgO-free}}$) is 60% and 23.6% in the field of $H = 100$ Oe for nanowire MgO-added and nanoparticle MgO-added composites, respectively. As the temperature drops to 50 K, the enhancements of magnetization reach 180.2% and 89.02% for nanowire MgO-added and nanoparticle MgO-added composites, respectively. To explore the difference in low-field magnetization further, the magnetizations as a function of magnetic field were measured at 5 K and the typical results are shown in figure 6(*b*). It shows that the magnetization of the P-LCMO and W-LCMO composites is larger than that of the MgO-free LCMO in the low field range below 7 kOe, while it is smaller in the field as high as 50 kOe as shown in figure 6(*b*). These results indicate that the addition of nano-MgO to LCMO composites would enhance the sensitivity to magnetization in low magnetic field, which is valuable from the viewpoint of applications.

Figure 7 presents MR (defined as $MR = [\rho(H) - \rho(0T)]/\rho(0T)$) as a function of external magnetic field H at $T = 100$ K for the series of samples. It demonstrates that the LFMR values of P-LCMO and W-LCMO samples are larger than that of pure LCMO in the low field range below 2 kOe. Moreover, for the W-LCMO sample, the LFMR is significantly enhanced 1.3 times that of P-LCMO at 2 kOe. This enhanced LFMR of nano-MgO added LCMO composites can be similarly interpreted by the mechanism of spin-polarized tunnelling through manganite/insulator/manganite junction structure, which has been widely used in the papers [4–8]. At temperatures below T_{C2}, the FM LCMO particles are embedded in the nonmagnetic MgO. Under a small external field, magnetic domains rotate towards one orientation and spin-polarized tunnelling through the LCMO/MgO/LCMO junction structure contributes to the enhancement of LFMR at low temperatures. On the other hand, the larger enhancement of LFMR in W-LCMO composites than that in P-LCMO may be ascribed to the larger aspect ratio and more efficient dispersal of MgO. Our results imply that the morphology of added insulating materials can affect their distribution across the grain boundaries of CMR materials and LFMR.

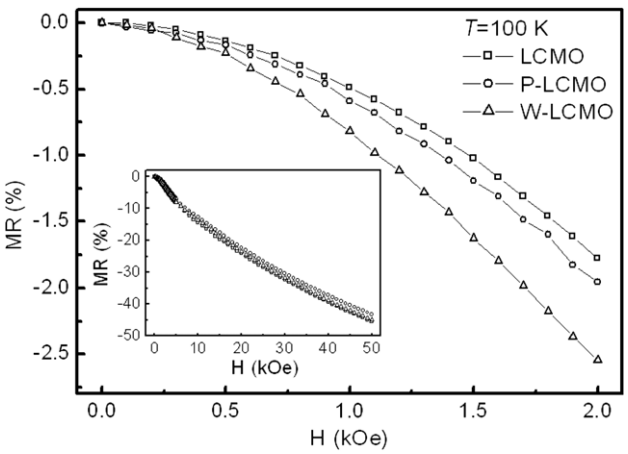

Figure 7. LFMR of nano-MgO added LCMO composites as functions of external field H at $T = 100$ K. The inset shows *MR(H)* in the field range of $0 < H < 50$ kOe.

Finally, we consider the high field MR response. Comparison of the data in the inset of figure 7 reveals that the slope of $MR(H)$ in the 5 kOe $< H <$ 50 kOe field region is identical for all the samples. That is to say, the high field MR does not depend on the addition of nano-MgO. This result implies that the high field response is not related to the intergrain coupling but reflects the magnetic and electric characteristics of the LCMO grains themselves.

4. Conclusion

In summary, the effect of nano-MgO addition on the transport and magnetic properties of LCMO is investigated. It is found that the magnetization of the nano-MgO added compounds is highly sensitive to a low applied field below 7 kOe compared with the MgO-free LCMO. In addition, the enhancement of low-field magnetoresistance is found in nano-MgO added compounds and the enhancement for the nanowire MgO-added composite is more remarkable than that for the nanoparticle MgO-added one. Moreover, two ferromagnetic phases with low-T_C and high-T_C in nano-MgO added compounds are observed. We attribute the additional FM transition to the 3D tensile strain due to the lattice mismatch between $La_{2/3}Ca_{1/3}MnO_3$and MgO. Our results imply that the low-field transport and magnetic properties in manganite/insulator/manganite polycrystalline samples can be manipulated further by controlling the morphology and the distribution of added insulating materials in the grain boundaries of manganite.

Acknowledgments

The authors would like to thank M G Kong for help during the experiments on FE-SEM. This work is supported by the National Key Basic Research under Contract No 2006CB601005, the National Nature Science Foundation of China under Contract Nos 10474100, 10374033 and 50672099 and the Director's Fund of the Hefei Institutes of Physical Science, Chinese Academy of Sciences.

References

[1] Coey J M D, Viret M and von Molnar S 1999 *Adv. Phys.* **48** 167 and references therein
[2] Siwach P K, Goutam U K, Srivastava P, Singh H K, Tiwari R S and Srivastava O N 2006 *J. Phys. D: Appl. Phys.* **39** 14–20

[3] Zhu X B, Yang J, Zhao B C, Sheng Z G, Liu S M, Lu W J, Song W H and Sun Y P 2004 *J. Phys. D: Appl. Phys.* **37** 2347
[4] Baleells Ll, Carrillo A E, Martinez B and Fontcuberta J 1999 *Appl. Phys. Lett.* **74** 4014
[5] Petrov D K, Krusin-Elbaum L, Sun J Z, Field C and Duncombe P R 1999 *Appl. Phys. Lett.* **75** 995
[6] Moshnyaga V *et al* 2003 *Nat. Mater.* **2** 247
[7] Hwang H Y, Cheong S-W, Ong N P and Battlog B 1996 *Phys. Rev. Lett.* **77** 2041
[8] Worledge D C and Geballe T H 2000 *Appl. Phys. Lett.* **76** 900
[9] Xia Y N, Yang P D, Sun Y G, Wu Y Y, Mayers B, Gates B, Yin Y D, Kim F and Yan H Q 2003 *Adv. Mater.* **15** 353
[10] Yan P, Ye C H, Fang X S, Zhao J W, Wang Z Y and Zhang L D 2005 *Chem. Lett.* **34** 384
[11] Ma Y Q, Song W H, Zhang R L, Dai J M, Yang J, Du J J, Sun Y P, Bi Z, Ge Y J and Qiu X G 2004 *Phys. Rev.* B **69** 134404
[12] Millis A J, Darling T and Migliori A 1998 *J. Appl. Phys.* **83** 1588
[13] Wang H S, Wertz E, Hu Y F, Li Q and Schlom D G 2000 *J. Appl. Phys.* **87** 7409